

Static polarizability of two-dimensional hole gases

Thomas Kernreiter¹, Michele Governale¹ and Ulrich Zülicke^{2,3}

¹School of Chemical and Physical Sciences and MacDiarmid Institute for Advanced Materials and Nanotechnology, Victoria University of Wellington, PO Box 600, Wellington 6140, New Zealand

²Institute of Fundamental Sciences and MacDiarmid Institute for Advanced Materials and Nanotechnology, Massey University, Manawatu Campus, Private Bag 11 222, Palmerston North 4442, New Zealand

³Centre for Theoretical Chemistry and Physics, Massey University, Albany Campus, Private Bag 102904, North Shore MSC, Auckland 0745, New Zealand

E-mail: thomas.kernreiter@vuw.ac.nz, michele.governale@vuw.ac.nz, u.zuelicke@massey.ac.nz

Abstract. We have calculated the density-density (Lindhard) response function of a homogeneous two-dimensional (2D) hole gas in the static ($\omega = 0$) limit. The bulk valence-band structure comprising heavy-hole (HH) and light-hole (LH) states is modeled using Luttinger's $\mathbf{k} \cdot \mathbf{p}$ approach within the axial approximation. We elucidate how, in contrast to the case of conduction electrons, the Lindhard function of 2D holes exhibits unique features associated with (i) the confinement-induced HH-LH energy splitting and (ii) the HH-LH mixing arising from the charge carriers' in-plane motion. Implications for the dielectric response and related physical observables are discussed.

PACS numbers: 71.10.-w, 71.70.Ej, 73.21.Fg

Submitted to: *New J. Phys.*

1. Introduction

The density-density response function is a very fundamental materials characteristics, as it determines a host of thermodynamic and transport properties in condensed-matter systems [1]. It has been discussed extensively within the paradigmatic model of the homogeneous electron gas [2] and studied for low-dimensional conductors realised in semiconductor heterostructures [3]. More recently, static and dynamic response properties of two-dimensional (2D) conduction-electron systems with spin-orbit coupling have been investigated in considerable detail [4–9]. This surge of interest arose partly because of important ramifications for possible spintronics applications [10, 11]. In contrast, very few studies have considered how the peculiar electronic properties of a typical semiconductor’s valence band [12] affect the polarizability and other many-body response functions of p -type semiconductor materials, and these existing works [13–15] have focused on bulk (3D) systems. As high-quality 2D holes gases have recently become available for experimental study, both in modulation-doped [16–20] and accumulation-layer [21] heterostructures, a detailed theoretical analysis of their many-body response properties is warranted. Here we provide such a study and show how the intricate interplay between quantum confinement and strong spin-orbit-coupled dynamics in the valence band [22] has a profound effect on the static polarizability.

Charge carriers from the conduction and valence bands of typical semiconductors exhibit profoundly different spin properties. Conduction electrons are quite ordinary in that they are spin-1/2 particles carrying a fixed intrinsic magnetic dipole moment, like free electrons in vacuum. Holes are different; they have an intrinsic spin-3/2 degree of freedom because valence-band states are strongly modified by spin-orbit coupling [12]. As a result, the orbital dynamics of holes in a bulk sample also depends on the magnitude of projection for their spin parallel to their direction of motion. States with spin-3/2 projection quantum number $m_J = \pm 3/2$ ($\pm 1/2$) are called heavy holes, HHs (light holes, LHs), because their band-energy dispersion has a smaller (larger) curvature. When holes are confined in a 2D heterostructure, the quantum-well growth direction is the natural spin-quantisation axis (taken to be the z direction in the following), and the difference in effective masses translates into an energy splitting between the HH and LH subband edges corresponding to the same transverse orbital bound state [23]. As the in-plane motion couples HH and LH states, 2D holes with finite wave vector $\mathbf{k}_{\parallel} = (k_x, k_y)$ are no longer of purely HH or LH type [22, 23]. While the HH-LH (subband-edge) splitting is easily accounted for and usually included in theoretical analyses, the HH-LH *mixing* has sometimes been ignored. It may be tempting to make such a simplification, given that the density of typical 2D hole gases is quite often low enough that only the lowest (HH-like) subband is occupied. However, detailed analysis shows this approach to be too crude for most relevant situations [22]. Even only qualitatively accurate predictions basically always require the inclusion of HH-LH mixing alongside the HH-LH splitting. As we will show below, the density-density response of 2D hole gases is strongly affected by HH-LH mixing, i.e., is not simply the sum of the response functions of independent

2D (HH and LH) gases.

This article is organised as follows. In Section 2, we introduce our model for the upper-most valence band of typical semiconductors, which is based on the Luttinger Hamiltonian [24, 25] in axial approximation [22, 26, 27]. The definition and basic calculational details for the density-density (Lindhard) response function are given in Sec. 3, including analytical results pertaining to the 2D hole gas in certain limits. We present plots of the numerically determined static polarizability in Sec. 4 and discuss basic features. Our conclusions are given in Sec. 5.

2. Luttinger-model description of a 2D hole system

The Luttinger model [25] provides a useful description of the upper-most valence band of typical semiconductors in situations where its couplings to the conduction band and split-off valence band are irrelevant. We adopt this model here to investigate how the many-body physics of 2D holes is affected by their peculiar spin-3/2 properties. In principle, more extended [27, 28] multiband Hamiltonians could be employed to improve the accuracy of quantitative predictions. However, to illustrate the qualitatively new features exhibited by 2D hole gases in contrast to their conduction-electron counterparts, the Luttinger-model description is adequate. The particular geometry for our case of interest suggests using, as our starting point, the Luttinger-model Hamiltonian H_L in *axial* approximation [22, 26, 27]:

$$H_L = H_0 + H_1 + H_2 \quad , \quad (1a)$$

$$H_0 = -\frac{\hbar^2}{2m_0} \left[\gamma_1 (\mathbf{k}_{\parallel}^2 + k_z^2) + \tilde{\gamma}_1 (\mathbf{k}_{\parallel}^2 - 2k_z^2) \left(\hat{J}_z^2 - \frac{5}{4} \hat{1} \right) \right] \quad , \quad (1b)$$

$$H_1 = \frac{\hbar^2}{m_0} \sqrt{2} \tilde{\gamma}_2 \left(\{k_z, k_+\} \{ \hat{J}_z, \hat{J}_- \} + \{k_z, k_-\} \{ \hat{J}_z, \hat{J}_+ \} \right) \quad , \quad (1c)$$

$$H_2 = \frac{\hbar^2}{2m_0} \tilde{\gamma}_3 \left(k_+^2 \hat{J}_-^2 + k_-^2 \hat{J}_+^2 \right) \quad . \quad (1d)$$

Cartesian components of the spin-3/2 matrix vector are denoted by $\hat{J}_{x,y,z}$, and we used the abbreviations $k_{\pm} = k_x \pm ik_y$, $\hat{J}_{\pm} = (\hat{J}_x \pm i\hat{J}_y)/\sqrt{2}$, and $\{A, B\} = (AB + BA)/2$. The constants γ_1 and $\tilde{\gamma}_j$ are materials-dependent bandstructure parameters [29]. Note that the $\tilde{\gamma}_j$ depend also on the quantum-well growth direction; their explicit expressions in terms of the standard Luttinger parameters [25, 29] γ_2 and γ_3 can be found, e.g., in Table C.10 of Ref. [22].

The dynamics of holes confined in a 2D quantum well is modeled by the Hamiltonian $H_L + V(z)$. In the following, we assume the external potential $V(z)$ to be a hard-wall confinement of width d and consider only its lowest size-quantised orbital bound state. An effective Hamiltonian describing the 2D hole gas is then obtained from (1a) by replacing $k_z \rightarrow \langle k_z \rangle = 0$ and $k_z^2 \rightarrow \langle k_z^2 \rangle = (\pi/d)^2$. Introducing the energy scale $E_0 = \pi^2 \hbar^2 \gamma_1 / (2m_0 d^2)$ and measuring wave vectors in units of π/d , the 2D hole-gas

Hamiltonian is given by

$$H_L^{(2D)} = H_0^{(2D)} + H_{\text{mix}} \quad , \quad (2a)$$

$$H_0^{(2D)} = -E_0 \left\{ 1 - 2\bar{\gamma} \left(\hat{J}_z^2 - \frac{5}{4} \hat{1} \right) + \left[1 + \bar{\gamma} \left(\hat{J}_z^2 - \frac{5}{4} \hat{1} \right) \right] \bar{\mathbf{k}}_{\parallel}^2 \right\} \quad , \quad (2b)$$

$$H_{\text{mix}} = E_0 \alpha \bar{\gamma} \left(\bar{k}_+^2 \hat{J}_-^2 + \bar{k}_-^2 \hat{J}_+^2 \right) \quad . \quad (2c)$$

Here $\bar{k}_{x,y} = k_{x,y} d/\pi$, $\bar{\gamma} = \tilde{\gamma}_1/\gamma_1$, and $\alpha = \tilde{\gamma}_3/\tilde{\gamma}_1$. We are using the parameterisation in terms of $\bar{\gamma}$ and α to be able to separately discuss the effects of HH-LH splitting, which is embodied in $H_0^{(2D)}$, and HH-LH mixing arising from H_{mix} .

Diagonalising $H_L^{(2D)}$ from (2a) yields in-plane dispersion relations $E_j(\mathbf{k}_{\parallel}) = -E_0 \varepsilon_{\mathbf{k}_{\parallel}}^{(j)}$ with $j = 1, \dots, 4$ and

$$\varepsilon_{\mathbf{k}_{\parallel}}^{(j)} = 1 + \bar{k}_x^2 + \bar{k}_y^2 + \sigma_j \bar{\gamma} \sqrt{(\bar{k}_x^2 + \bar{k}_y^2 - 2)^2 + 3\alpha^2(\bar{k}_x^2 + \bar{k}_y^2)^2} \quad . \quad (3)$$

Here $\sigma_1 = \sigma_2 = -\sigma_3 = -\sigma_4 = 1$. Using the result (3), we obtain the two dimensionless Fermi wave vectors

$$\bar{k}_{F1,2} = \left[\frac{\varepsilon_F - 1 - 2\bar{\gamma}^2 \mp \bar{\gamma} \sqrt{(\varepsilon_F - 3)^2 + 3\alpha^2[(\varepsilon_F - 1)^2 - 4\bar{\gamma}^2]}}{1 - \bar{\gamma}^2(1 + 3\alpha^2)} \right]^{\frac{1}{2}} \quad , \quad (4)$$

in terms of the dimensionless Fermi energy $\varepsilon_F = -E_F/E_0$. The 2D-hole sheet density n_{2D} is related to the dimensionless Fermi wave vectors according to

$$n_{2D} = \left(\frac{\pi}{d} \right)^2 \frac{\bar{k}_{F1}^2 \Theta(\varepsilon_F - [1 + 2\bar{\gamma}]) + \bar{k}_{F2}^2 \Theta(\varepsilon_F - [1 - 2\bar{\gamma}])}{2\pi} \quad , \quad (5)$$

where $\Theta(x)$ denotes the Heaviside step function.

The eigenvectors $|\chi_{\mathbf{k}_{\parallel}}^{(j)}\rangle$ corresponding to eigenvalues $E_j(\mathbf{k}_{\parallel})$ of $H_L^{(2D)}$ can be straightforwardly determined. For $j = 1, 2$ and in the basis representation where \hat{J}_z is diagonal, we find

$$|\chi_{\mathbf{k}_{\parallel}}^{(1)}\rangle = \begin{pmatrix} 0 \\ \frac{(s-t)(\bar{k}_x - i\bar{k}_y)^2}{\bar{k}_{\parallel}^2 \sqrt{(s-t)^2 + 3\alpha^2 \bar{k}_{\parallel}^4}} \\ 0 \\ \frac{\sqrt{3}\alpha \bar{k}_{\parallel}^2}{\sqrt{(s-t)^2 + 3\alpha^2 \bar{k}_{\parallel}^4}} \end{pmatrix}, \quad |\chi_{\mathbf{k}_{\parallel}}^{(2)}\rangle = \begin{pmatrix} \frac{(-s-t)(\bar{k}_x - i\bar{k}_y)^2}{\bar{k}_{\parallel}^2 \sqrt{(-s-t)^2 + 3\alpha^2 \bar{k}_{\parallel}^4}} \\ 0 \\ \frac{\sqrt{3}\alpha \bar{k}_{\parallel}^2}{\sqrt{(-s-t)^2 + 3\alpha^2 \bar{k}_{\parallel}^4}} \\ 0 \end{pmatrix}, \quad (6)$$

with $s \equiv \bar{k}_{\parallel}^2 - 2$ and $t \equiv \sqrt{s^2 + 3\alpha^2 \bar{k}_{\parallel}^4}$. The remaining eigenspinors $|\chi_{\mathbf{k}_{\parallel}}^{(3)}\rangle$ and $|\chi_{\mathbf{k}_{\parallel}}^{(4)}\rangle$ are obtained by changing $t \rightarrow -t$ in $|\chi_{\mathbf{k}_{\parallel}}^{(1)}\rangle$ and $|\chi_{\mathbf{k}_{\parallel}}^{(2)}\rangle$, respectively. As the scalar products $\langle \chi_{\mathbf{k}_{\parallel}}^{(j)} | \chi_{\mathbf{k}_{\parallel}+\mathbf{q}}^{(l)} \rangle$ enter in the calculation of the Lindhard function, we briefly discuss their relevant properties. The moduli $|\langle \chi_{\mathbf{k}_{\parallel}}^{(j)} | \chi_{\mathbf{k}_{\parallel}+\mathbf{q}}^{(j)} \rangle|$ are found to be equal for all $j = 1, \dots, 4$. Also, $|\langle \chi_{\mathbf{k}_{\parallel}}^{(j)} | \chi_{\mathbf{k}_{\parallel}+\mathbf{q}}^{(l)} \rangle|$ are pairwise the same for $(j, l) = (1, 3)$ and $(3, 1)$; and $(j, l) = (2, 4)$ and $(4, 2)$. These relations can be verified using the explicit form of the column vectors in (6) together with the fact that the eigenspinors satisfy orthonormality relations.

3. Lindhard function of a 2D hole gas: General expression and special cases

The general definition [2] of the Lindhard function, specialised to a 2D system, reads

$$\chi(\omega, \mathbf{q}) = \lim_{\delta \rightarrow 0} \sum_{j,l=1}^4 \int \frac{d^2 k_{\parallel}}{(2\pi)^2} |\langle \chi_{\mathbf{k}_{\parallel}}^{(j)} | \chi_{\mathbf{k}_{\parallel}+\mathbf{q}}^{(l)} \rangle|^2 \frac{n_F[E_j(\mathbf{k}_{\parallel})] - n_F[E_l(\mathbf{k}_{\parallel} + \mathbf{q})]}{\hbar\omega + i\delta + E_j(\mathbf{k}_{\parallel}) - E_l(\mathbf{k}_{\parallel} + \mathbf{q})} \quad , \quad (7)$$

with $n_F(E)$ denoting the Fermi-Dirac distribution function. The expression given in (7) can be simplified by using a polar-coordinate representation where $k_x = k_{\parallel} \cos \phi$ and $k_y = k_{\parallel} \sin \phi$ and performing a change of variables in the terms involving $n_F[E_j(\mathbf{k}_{\parallel} + \mathbf{q})]$ such that $\mathbf{k}_{\parallel} \rightarrow \mathbf{k}_{\parallel} - \mathbf{q}$ and $\phi \rightarrow \phi + \pi$, which leaves the energy difference and the spinor overlap invariant. Using also the description in terms of dimensionless quantities and specialising to the zero-temperature limit, the Lindhard function can be expressed as $\chi(\omega, \mathbf{q}) = -(2m_0/\hbar^2\gamma_1) \bar{\chi}(\bar{\omega}, \bar{q})$, with

$$\bar{\chi}(\bar{\omega}, \bar{q}) = \lim_{\delta \rightarrow 0} \sum_{\eta=\pm 1} \sum_{j,l=1}^4 \int_0^{\bar{K}_{F_j}} \bar{k}_{\parallel} d\bar{k}_{\parallel} \int_0^{2\pi} \frac{d\phi}{(2\pi)^2} \frac{|\langle \chi_{\bar{\mathbf{k}}_{\parallel}}^{(j)} | \chi_{\bar{\mathbf{k}}_{\parallel}+\bar{\mathbf{q}}}^{(l)} \rangle|^2}{\eta(\bar{\omega} + i\delta) + \varepsilon_{\bar{\mathbf{k}}_{\parallel}}^{(j)} - \varepsilon_{\bar{\mathbf{k}}_{\parallel}+\bar{\mathbf{q}}}^{(l)}} \quad . \quad (8)$$

We use a notation where $\bar{K}_{F_1} = \bar{K}_{F_2} \equiv \bar{k}_{F_1}$, $\bar{K}_{F_3} = \bar{K}_{F_4} \equiv \bar{k}_{F_2}$, and $\bar{\omega} = \hbar\omega/E_0$. Note that, because the Luttinger Hamiltonian in axial approximation exhibits rotational invariance of in-plane hole motion, the Lindhard function depends on wave vector \mathbf{q} only via its (dimensionless) magnitude \bar{q} . Also, within our effective 2D description, $\chi(\omega, \mathbf{q})$ is independent of the quantum-well width d and inversely proportional to γ_1 .

In the following, we consider the static limit, which is obtained by setting $\bar{\omega} = 0$. Specialising further to certain limiting situations, we can find analytical expressions for the Lindhard function. For example, for the case of vanishing HH-LH mixing obtained by letting $\alpha \rightarrow 0$, the matrix $|\langle \chi_{\bar{\mathbf{k}}_{\parallel}}^{(j)} | \chi_{\bar{\mathbf{k}}_{\parallel}+\bar{\mathbf{q}}}^{(l)} \rangle|^2$ of modulus-squared scalar products reduces to the unity matrix, and the simple analytical expression

$$\bar{\chi}(0, \bar{q})|_{\alpha=0} = \frac{-1}{2\pi\bar{q}} \sum_{j=1}^2 \left\{ \frac{\Theta(\bar{k}_{F_j})}{1 - \sigma_j\bar{\gamma}} \left[\bar{q} - \sqrt{\bar{q}^2 - 4\bar{k}_{F_j}^2} \Theta\left(\frac{\bar{q}}{2\bar{k}_{F_j}} - 1\right) \right] \right\} \quad , \quad (9)$$

is found, where $\sigma_1 = -\sigma_2 = 1$. Inspection of the result (9) shows that, with only HH-LH splitting included, the static Lindhard function comprises two separate HH and LH contributions, each being the standard 2D-electron-gas expression [2] with Fermi wave vector and effective mass adjusted to the respective HH and LH values. On the other hand, taking the limit $\bar{\mathbf{q}} \rightarrow 0$ in (8), the matrix of modulus-squared spinor overlaps again becomes the unity matrix, and we find an analytical result for the (dimensionless) density of states at the Fermi energy,

$$\lim_{\bar{q} \rightarrow 0} \bar{\chi}(0, \bar{q}) = \frac{-1}{2\pi} \sum_{j=1}^2 \Theta(\bar{k}_{F_j}) \left| 1 - \sigma_j\bar{\gamma} \frac{2 - \bar{k}_{F_j}^2(1 + 3\alpha^2)}{\sqrt{(2 - \bar{k}_{F_j}^2)^2 + 3\alpha^2\bar{k}_{F_j}^4}} \right|^{-1} \quad . \quad (10)$$

Thus we see that one effect of HH-LH mixing is to introduce an energy (and concomitant density) dependence into the density of states of 2D holes.

4. Static polarizability of 2D holes: Numerical method and results

With analytical expressions unavailable for the Lindhard function (8) in the more general case with both \mathbf{q} and α finite, we have to resort to numerical calculations to investigate in greater detail how HH-LH mixing affects the static polarizability $\bar{\chi}(0, \bar{q})$. Note that the latter is an entirely real-valued function. The procedure for its numerical calculation is explained in the following Subsection, and our results are given thereafter.

4.1. Brief outline of the calculational method

For $\bar{\omega} = 0$, the integrand of (8) has poles whenever the energy difference in the denominator vanishes. These poles are regularised by the parameter δ , which needs to be set to zero after performing the integrations. We calculate these integrals numerically, taking special care in the regions close to values of the integration variables corresponding to a vanishing denominator. To identify the pole structure of the Lindhard function, we write the inverse of the energy difference as

$$\begin{aligned} \left(\varepsilon_{\bar{\mathbf{k}}_{\parallel}}^{(j)} - \varepsilon_{\bar{\mathbf{k}}_{\parallel} + \bar{\mathbf{q}}}^{(l)} \right)^{-1} &= (\delta_{j,1} + \delta_{j,2})(\delta_{l,1} + \delta_{l,2}) \frac{a_1 - b}{a_1^2 - b^2} \\ &+ (\delta_{j,1} + \delta_{j,2})(\delta_{l,3} + \delta_{l,4}) \frac{a_1 + b}{a_1^2 - b^2} \\ &+ (\delta_{j,3} + \delta_{j,4})(\delta_{l,1} + \delta_{l,2}) \frac{a_2 - b}{a_2^2 - b^2} \\ &+ (\delta_{j,3} + \delta_{j,4})(\delta_{l,3} + \delta_{l,4}) \frac{a_2 + b}{a_2^2 - b^2}, \end{aligned} \quad (11)$$

where $\delta_{j,l}$ denotes Kronecker's delta symbol. The quantities appearing in (11) are

$$a_{1,2} = \mp \bar{\gamma} \sqrt{4 - 4\bar{k}_{\parallel}^2 + (1 + 3\alpha^2)\bar{k}_{\parallel}^4 + \bar{q}^2 + \bar{k}_{\parallel}\bar{q} \cos \phi} \quad (12a)$$

$$b = \bar{\gamma} \sqrt{(-2 + \bar{k}_{\parallel}^2 + \bar{q}^2 + 2\bar{k}_{\parallel}\bar{q} \cos \phi)^2 + 3\alpha^2(\bar{k}_{\parallel}^2 + \bar{q}^2 + 2\bar{k}_{\parallel}\bar{q} \cos \phi)^2}. \quad (12b)$$

The denominators in (11) can be written as

$$\frac{1}{a_{1,2}^2 - b^2} = \frac{1}{4\bar{k}_{\parallel}^2\bar{q}^2[1 - (1 + 3\alpha^2)\bar{\gamma}^2]} \frac{1}{X_{1,2} - Y_{1,2}} \left(\frac{1}{\cos \phi - X_{1,2}} - \frac{1}{\cos \phi - Y_{1,2}} \right), \quad (13)$$

with the positions of the poles given by

$$\begin{aligned} X_{1,2} &= -\frac{\bar{q}}{2\bar{k}_{\parallel}}, \\ Y_{1,2} &= \frac{\pm 2\bar{\gamma} \sqrt{4 - 4\bar{k}_{\parallel}^2 + (1 + 3\alpha^2)\bar{k}_{\parallel}^4 - \bar{q}^2 + \bar{\gamma}^2[(2 + 6\alpha^2)\bar{k}_{\parallel}^2 - 4 + \bar{q}^2 + 3\alpha^2\bar{q}^2]}}{2\bar{k}_{\parallel}\bar{q}[1 - (1 + 3\alpha^2)\bar{\gamma}^2]}. \end{aligned} \quad (14)$$

As can be seen from (13), poles are encountered in the integration over ϕ when $|X_{1,2}|, |Y_{1,2}| \leq 1$. We have employed a Cauchy principle-value integration to regularise the Lindhard function in the vicinity of the poles specified in (14).

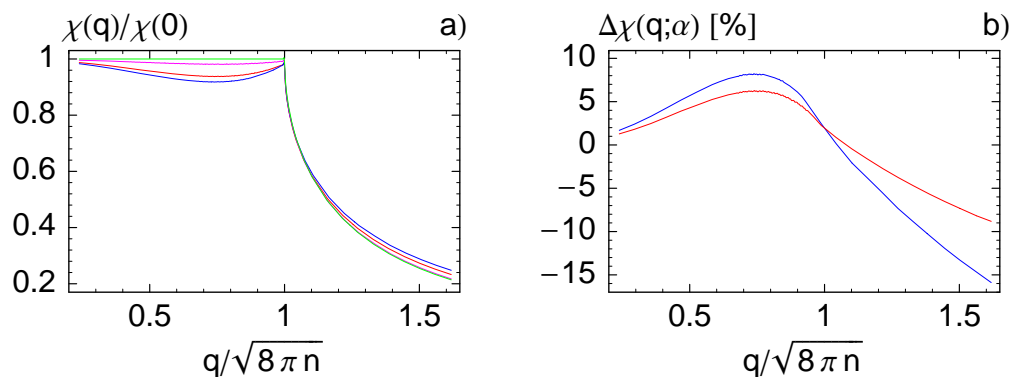


Figure 1. (a) Normalised Lindhard function $\chi(q)$ for the static limit and (b) the quantity $\Delta\chi(q; \alpha)$ that measures the impact of HH-LH mixing (see text), plotted as a function of wave-vector magnitude q . The blue curve is for $\bar{\gamma} = 0.31$ and $\alpha = 1.2$, which are parameter values applying to an [001]-grown heterostructure in GaAs. For comparison, results are also shown for $\alpha = 1$ (red curve), 0.5 (magenta curve), and 0 (green curve). For all cases, a value $\bar{n} = 0.0608$ for the dimensionless 2D hole density was used.

4.2. Results for model parameters applying to an [001] quantum well in GaAs

High-quality 2D hole gases have recently been fabricated from [001]-grown GaAs heterostructures [16, 17, 20]. To obtain results applicable to these systems, we use the appropriate model parameters $\bar{\gamma} = 0.31$ and $\alpha = 1.2$. Results for this configuration are presented below. For comparison and to clearly show the impact of HH-LH mixing, we also show results for the static polarizability when $\alpha = 1, 0.5$, and 0. In all these cases, we limit ourselves to the low-density regime where only the highest, HH-like, 2D subband is occupied. The reason for this caution is the fact that, within our model using a hard-wall confinement, the spectrum of all other than the highest subband poorly matches that of the real GaAs sample. To be specific, we choose $\bar{n} = 0.0608$. Recalling that the 2D-hole sheet density is related to the dimensionless density by $n = (\pi/d)^2 \bar{n}$, this value would correspond to a density of $n = 1.5 \times 10^{15} \text{ m}^{-2}$ in a 20-nm quantum well.

To avoid cluttering our notation, we suppress the zero-frequency argument in the formal expression of the static Lindhard function from now on: $\chi(0, \mathbf{q}) \equiv \chi(q)$. In Figure 1(a), we plot $\chi(q)/\chi(0)$ as a function of $q/\sqrt{8\pi n}$, for different values of the parameter α that quantifies the HH-LH mixing. It is apparent that a finite α leads to a significant suppression of $\chi(q)$ below the constant-plateau value usually associated with 2D systems [2] for $q < \sqrt{8\pi n}$. To make the impact of HH-LH mixing quantitatively explicit, we define the variable

$$\Delta\chi(q; \alpha) = 1 - \frac{\chi(q)}{\chi(0)} \bigg|_{\alpha} \left[\frac{\tilde{\chi}(q)}{\tilde{\chi}(0)} \bigg|_{\alpha} \right]^{-1}, \quad (15)$$

where $\tilde{\chi}(q)$ is the analytical result (9) obtained for the limit $\alpha = 0$ but with Fermi wave vectors adjusted to coincide with those found in the case of the finite α under consideration. Thus the function $\Delta\chi(q; \alpha)$ measures the relative change exhibited in

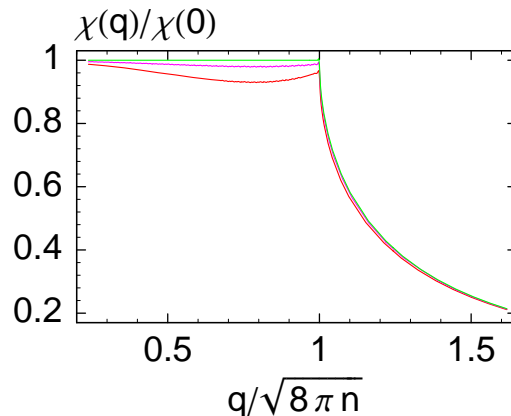


Figure 2. Normalised Lindhard function $\chi(q)$ for the low-density regime of a fictitious semiconductor material with $\bar{\gamma} = 0.2$ and (dimensionless) density $\bar{n} = 0.0608$. The red, magenta, and green curves correspond to $\alpha = 1, 0.5,$ and 0 , respectively.

the normalised static polarizability that is due to a finite α but goes beyond a simple renormalisation of Fermi wave vectors.‡ In Figure 1(b), we show $\Delta\chi(q; \alpha)$ for $\alpha = 1$ (red curve) and $\alpha = 1.2$ (blue curve). It shows a strong variation as a function of $q/\sqrt{8\pi n}$ and reaches the 10% level.

4.3. Results for a model semiconductor: High- and low-density regimes

For high-enough 2D densities, holes will occupy both the HH-like and LH-like subbands arising from the lowest-energy orbital bound state in the quantum well. It can be expected that this high-density regime is qualitatively different from the situation at low density where only the highest (HH-like) 2D subband is occupied. To treat the case of high density consistently within our adopted model, it needs to be ensured that the LH-like subband arising from the lowest-energy orbital bound state is still higher in energy than the HH-like subband associated with the next orbital-bound-state level. For a hard-wall confinement considered here, a system with $\bar{\gamma} = 0.2$ satisfies that condition. Although this value does not directly correspond to a specific semiconductor material, we use it to illustrate the generically different impact of HH-LH mixing in the low and high-density regimes, respectively.

To provide a clear benchmark for comparing high and low-density regimes, we start by presenting the result for the low density case ($\bar{n} = 0.0608$, same value as used in the calculations for Figure 1) in Figure 2. The obtained curves look qualitatively similar to those found for the low-density regime in GaAs (different $\bar{\gamma}$, shown in Figure 1), but the quantitative level of suppression below the plateau value obtained in the limit of vanishing α is different here.

‡ In the low-density limit considered here, there is only one Fermi wave vector whose magnitude is the same for all values of α , and $\tilde{\chi}(q)$ actually coincides with $\chi(q)|_{\alpha=0}$. However, as we will see further below, $\tilde{\chi}(q) \neq \chi(q)|_{\alpha=0}$ in the more general case when both the HH and LH subbands arising from the lowest 2D orbital bound state are occupied and, thus, two Fermi wave vectors exist.

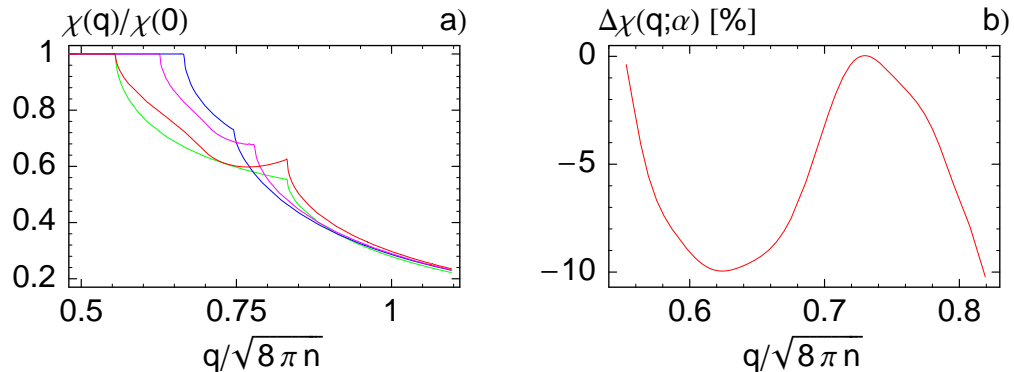


Figure 3. (a) Normalised Lindhard function $\chi(q)$ for the static limit and (b) the quantity $\Delta\chi(q; \alpha)$ that measures the impact of HH-LH mixing (see text), for the case with $\bar{\gamma} = 0.2$ and (dimensionless) density $\bar{n} = 0.4055$, corresponding to the high-density regime with both HH-like and LH-like 2D subbands occupied. The red, magenta, and blue curves are obtained for $\alpha = 1, 0.5$, and 0 , respectively. For comparison, we also plot (as the green curve) the analytical result (9) with Fermi-wave-vector values adjusted to coincide with the $\alpha = 1$ case. Therefore, the red and green curves in panel (a) exhibit kink-like features at the same values of q , and deviations between the two illustrate the effect of HH-LH mixing beyond a simple renormalisation of the Fermi wave vectors.

As an illustration of the high-density regime, we present results for $\bar{n} = 0.4055$, which would correspond to $n = 10^{16} \text{ m}^{-2}$ in a 20-nm quantum well. The normalised Lindhard function for this case is plotted in Figure 3(a). Note that, for the three values of α for which results are presented, the two Fermi wave vectors are different, see (4). As a result, the sharp features arising in the Lindhard function from poles at $-q/2k_{F_{1,2}}$ appear at different values of q in each curve. In contrast to the low-density case, a plateau is again exhibited in the static Lindhard function (for $q \leq 2k_{F_1}$). To illustrate effects due to HH-LH mixing beyond a simple renormalisation of the two Fermi wave vectors, we also show (as the green curve) the analytical result (9) for the Lindhard function in the limit $\alpha = 0$ but with values for the Fermi wave vectors taken from the case $\alpha = 1$. The latter result corresponds to that expected for two independent 2D hole gases with different Fermi wave vectors. Thus, any deviation between the red and green curves is entirely due to the mixed HH-LH character of 2D hole states. Figure 3(b) shows the corresponding difference function $\Delta\chi(q; \alpha)$ for $\alpha = 1$. Again, HH-LH mixing appears to cause differences around the 10%-level.

5. Summary and Conclusions

We have calculated the density-density response function of a homogeneous 2D hole gas in the static limit, based on the Luttinger-model description of the upper-most valence band within the axial approximation. While this approach neglects the warping of energy dispersions (and, hence, Fermi surfaces) for the holes' in-plane motion due to the cubic crystal symmetry, it already captures essential new features arising from the

peculiar valence-band properties. We furthermore focused only on the lowest orbital bound state in a symmetric quantum well defined by a hard-wall confinement. HH-LH splitting gives rise to the existence of two energetically separated 2D hole subbands, one (at higher energy) mostly HH-like and the other of mostly LH character. However, except for states with zero in-plane kinetic energy, HH and LH amplitudes are mixed, and we have elucidated how this mixing gives rise to marked changes in the shape and magnitude of the static density response function. New analytical results are derived for the limit $q \rightarrow 0$, but the case with finite q and HH-LH mixing included could only be treated numerically.

Both for practical and theoretical reasons, it makes sense to distinguish two basic situations. One corresponds to the low-density regime where only the highest (mostly HH-like) 2D subband is occupied. In this limit, our model can be expected to describe real semiconductor heterostructures quite accurately, even quantitatively, if adequate band-structure parameters are used as input to our calculations. As it turns out, even though holes are present only in the HH-like 2D subband, HH-LH mixing importantly affects the static density response. In particular, the response function is suppressed below the plateau exhibited by the standard 2D-electron-gas result [2], as illustrated in Figures 1(a) and 2. In the high-density regime, where both the HH-like and LH-like 2D subbands associated with the lowest-energy quantum-well bound state are occupied, the density response differs from that expected for two independent 2D hole gases. Thus HH-LH mixing is shown to influence the Lindhard function beyond a trivial renormalisation of Fermi-wave-vector magnitudes. We have defined, and calculated, the quantity $\Delta\chi(q; \alpha)$ to make the nontrivial effects arising from HH-LH mixing quantitatively explicit. For the parameters considered, relative changes on the order of 10% are seen.

In this work, we employed the approximation of hard-wall (infinite-height) quantum-well barriers. In the more realistic case of finite-height barriers, the HH and LH bound-state wave functions will both penetrate into the barrier regions. Due to HH-LH splitting, the range of penetration will be higher for LH states, i.e., the effective quantum-well width will be larger for LHs. This subtle difference between HH and LH bound states scales with the parameter $\bar{\gamma}$ and can be expected to result in corrections of order $\alpha\bar{\gamma}^2$ to effects due to HH-LH mixing.

The qualitative and quantitative impact of HH-LH mixing can be expected to affect physical properties of 2D hole gases in an important way and, thus, render their behaviour quite different from that exhibited by 2D conduction-electron systems. Examples for physical observables that are affected include the shape and range of Friedel oscillations exhibited by 2D hole gases in response to impurity charges present, e.g., in the doping layer of modulation-doped heterostructures. HH-LH mixing should then also influence the 2D-hole-mediated Ruderman-Kittel-Kasuya-Yosida (RKKY) interaction between magnetic impurities. A detailed investigation of this effect could shed new light on how to tailor the ferromagnetic properties of 2D diluted-magnetic-semiconductor heterostructures [30–34].

References

- [1] Ziman J M 1972 *Theory of Solids* 2nd ed (Cambridge, UK: Cambridge U Press)
- [2] Giuliani G and Vignale G 2005 *Quantum Theory of the Electron Liquid* (Cambridge, UK: Cambridge U Press)
- [3] Ando T, Fowler A B and Stern F 1982 *Rev. Mod. Phys.* **54** 437
- [4] Chen G H and Raikh M E 1999 *Phys. Rev. B* **59** 5090
- [5] Wang X F 2005 *Phys. Rev. B* **72** 085317
- [6] Farid A K and Mishchenko E G 2006 *Phys. Rev. Lett.* **97** 096604
- [7] Pletyukhov M and Gritsev V 2006 *Phys. Rev. B* **74** 045307
- [8] Badalyan S M, Matos-Abiague A, Vignale G and Fabian J 2009 *Phys. Rev. B* **79** 205305
- [9] Ambrosetti A, Pederiva F, Lipparini E and Gandolfi S 2009 *Phys. Rev. B* **80** 125306
- [10] Zutić I, Fabian J and Sarma S D 2004 *Rev. Mod. Phys.* **76** 323
- [11] Awschalom D D and Flatté M E 2006 *Nat. Phys.* **3** 153
- [12] Yu P Y and Cardona M 1999 *Fundamentals of Semiconductors* 2nd ed (Berlin: Springer)
- [13] Schliemann J 2006 *Phys. Rev. B* **74** 045214
- [14] Stanescu T D and Galitski V 2006 *Phys. Rev. B* **74** 205331
- [15] Schliemann J The dielectric function of the semiconductor hole gas preprint arXiv:1003.4820
- [16] Grbić B, Ellenberger C, Ihn T, Ensslin K, Reuter D and Wieck A D 2004 *Appl. Phys. Lett.* **85** 2277
- [17] Manfra M J, Pfeiffer L N, West K W, de Picciotto R and Baldwin K W 2005 *Appl. Phys. Lett.* **86** 162106
- [18] Fischer F, Schuh D, Bichler M, Abstreiter G, Grayson M and Neumaier K 2005 *Appl. Phys. Lett.* **86** 192106
- [19] Schmult S, Gerl C, Wurstbauer U, Mitzkus C and Wegscheider W 2005 *Appl. Phys. Lett.* **86** 202105
- [20] Gerl C, Schmult S, Tranitz H P, Mitzkus C and Wegscheider W 2005 *Appl. Phys. Lett.* **86** 252105
- [21] Clarke W R, Micolich A P, Hamilton A R, Simmons M Y, Muraki K and Hirayama Y 2006 *J. Appl. Phys.* **99** 023707
- [22] Winkler R 2003 *Spin-Orbit Coupling Effects in Two-Dimensional Electron and Hole Systems* (Berlin: Springer)
- [23] Bastard G, Brum J A and Ferreira R 1991 *Solid State Physics* vol 44 ed H Ehrenreich and D Turnbull (San Diego: Academic Press) pp 229–415
- [24] Luttinger J M and Kohn W 1955 *Phys. Rev.* **97** 869
- [25] Luttinger J M 1956 *Phys. Rev.* **102** 1030
- [26] Suzuki K and Hensel J C 1974 *Phys. Rev. B* **9** 4184
- [27] Trebin H R, Rössler U and Ranvaud R 1979 *Phys. Rev. B* **20** 686
- [28] Mayer H and Rössler U 1991 *Phys. Rev. B* **44** 9048
- [29] Vurgaftman I, Meyer J R and Ram-Mohan L R 2001 *J. Appl. Phys.* **89** 5815
- [30] Haury A, Wasiela A, Arnoult A, Cibert J, Tatarenko S, Dietl T and Merle d'Aubigné Y 1997 *Phys. Rev. Lett.* **79** 511
- [31] Wojtowicz T, Lim W L, Liu X, Dobrowolska M, Furdyna J K, Yu K M, Walukiewicz W, Vurgaftman I and Meyer J R 2003 *Appl. Phys. Lett.* **83** 4220
- [32] Nazmul A M, Sugahara S and Tanaka M 2003 *Phys. Rev. B* **67** 241308
- [33] Nazmul A M, Amemiya T, Shuto Y, Sugahara S and Tanaka M 2005 *Phys. Rev. Lett.* **95** 017201
- [34] Wurstbauer U and Wegscheider W 2009 *Phys. Rev. B* **79** 155444